Application of classical nucleation theory to phase selection and composition of nucleated nanocrystals during crystallization of Co-rich (Co,Fe)-based amorphous precursors

P.R. Ohodnicki Jr. [a,*], D.E. Laughlin [a], M.E. McHenry [a], M. Widom [b]

[a] Materials Science and Engineering Department, Carnegie Mellon University, Pittsburgh, PA 15213, USA
[b] Physics Department, Carnegie Mellon University, Pittsburgh, PA 15213, USA

Abstract

Classical steady-state nucleation theory is applied to Co-rich Fe,Co-based alloys to provide a rationale for experimental observations during the nanocrystallization of Co-rich $(Co,Fe)_{89}Zr_7B_4$ and $(Co,Fe)_{88}Zr_7B_4Cu_1$ amorphous precursors. The amorphous precursor free energy is estimated using density functional theory. This simple theory suggests: (i) strain or interface energy effects could explain a tendency for a body-centered cubic (bcc) phase to form during crystallization. Dissolved glass formers (Zr,B) in crystalline phases may also contribute; (ii) similar face-centered cubic (fcc) and hexagonal close-packed (hcp) free energies could explain the presence of some hcp phase after crystallization even though fcc is stable at the crystallization temperature; (iii) nanocrystal compositions vary monotonically with the Co:Fe ratio of the amorphous precursor even when multiple phases are nucleating because nucleation is not dictated by the common tangency condition governing bulk phase equilibria; and (iv) Fe-enrichment of the bcc phase can be attributed to a relatively small free energy difference between the amorphous and bcc phases for high Co-containing alloys.
© 2010 Acta Materialia Inc. Published by Elsevier Ltd. All rights reserved.

Keywords: Crystallization; Nucleation; FeCo; Co-rich; Nanocomposite

1. Motivation and relevant experimental background

Fe- and Co-based soft magnetic nanocomposites are obtained by partial (primary) crystallization of an initially amorphous precursor to form a composite microstructure of Fe,Co-based nanocrystals embedded in a glass former enriched amorphous matrix [1–4]. The small grain size of the nanocomposite microstructure is critical for obtaining desirable soft magnetic properties [5]. Recent investigations of primary crystallization in high Co-containing $(Co,Fe)_{89}Zr_7B_4$ and $(Co,Fe)_{88}Zr_7B_4Cu_1$ nanocomposites have demonstrated large responses to magnetic field processing [6–10]. The similar free energies of body-centered cubic (bcc), face-centered cubic (fcc) and hexagonal close-

packed (hcp) phases also results in a more complex primary crystallization process than in corresponding Fe-rich alloys, where bcc-derivative structures are far more stable. Technically interesting magnetic properties were observed for Co-rich Co–Fe–Nb–Si–B- and Co–Fe–Zr–Si–B-based alloys [11–13], but we have focused on simpler $(Co,Fe)_{89}Zr_7B_4$ and $(Co,Fe)_{88}Zr_7B_4Cu_1$ alloys. Because of the relatively low solubility of Zr and B in bulk crystalline Fe,Co-alloys, we compared the phase identity of the nucleated nanocrystalline grains with predictions based on the bulk binary Fe–Co system [7,8,14].

The application of classical nucleation theory to these complex systems was inspired by recent work in understanding the phase selection of highly undercooled liquid droplets of simpler systems [15–20], as mentioned in our previous work [8]. The complex chemistries of the nanocomposites make a fully quantitative treatment intractable, and the goal

* Corresponding author. Tel.: +1 412 973 4416.
 E-mail address: paul.ohodnicki@gmail.com (P.R. Ohodnicki Jr.).

of this manuscript is to present general predictions for nucleation in Co-rich Fe,Co-based nanocomposite alloys using classical nucleation theory under a number of simplifying assumptions. The results are compared with interesting experimental observations reported in recent works [6–10,14], and we show that steady-state classical nucleation theory arguments can provide a rationale for them under realistic assumptions. This simple treatment should be viewed only as a starting point for understanding such complex systems. For example, a large body of recent work by Kelton et al. [21–24] questions the validity of classical nucleation theory for compositional partitioning systems where long-range diffusion in the parent phase is sluggish relative to the interfacial attachment rates of growing nuclei.

First we apply steady-state classical nucleation theory to free energy data for the binary Fe–Co system, an approach inspired by previous work aiming to understand the preferential nucleation of the bcc phase in a $(Co_{0.95}Fe_{0.05})_{89}Zr_7B_4$ alloy [14]. Using ab initio calculations justified by experimental data, we then semi-quantitatively supplement the binary Fe,Co free energies to gain insight into the importance of the free energy of the amorphous phase. Previous experimental observations of particular interest here include:

Observation 1. Preferential nucleation of the bcc phase with significantly higher Co contents than the composition corresponding to the intersection of the binary bcc and fcc free energy curves, X_{T_0}, at the crystallization temperature [6–8,14].

Observation 2. Multiple nanocrystalline phases present after crystallization, including bcc, fcc, and hcp for Fe:(Fe + Co) ratios lying within the single phase fcc region of the binary Fe–Co phase diagram at the crystallization temperature [6,9].

Observation 3. Monotonic variation in both the Fe:(Fe + Co) ratio and the lattice parameter of the crystalline phases for varying Fe:(Fe + Co) ratio of the amorphous precursor even when multiple crystalline phases are forming [6,8].

Observation 4. Fe-enrichment of the bcc phase for both Co-rich and near-equiatomic alloys [8,25].

2. Binary model

Classical nucleation theory states that the nucleus of a product phase, β, formed through thermal fluctuations must be larger than a critical size to spontaneously grow. Formation of a critical nucleus involves overcoming the activation barrier for nucleation, ΔG_β^*. ΔG_β^* and the steady-state nucleation rate, I_β, are expressed for a spherical precipitate as [26]:

$$\Delta G_\beta^* = \frac{16\pi\sigma_{\delta,\beta}^3}{3(\Delta G^\beta + W^{\delta,\beta})^2}, \quad I_\beta = K_\beta e^{\left(\frac{-\Delta G_\beta^*}{kT}\right)} \quad (1)$$

$\sigma_{\delta,\beta}$ is the interfacial free energy between the parent phase, δ, and the product phase, β. ΔG^β and $W^{\delta,\beta}$ are the thermodynamic driving force for formation of β-phase and the strain energy of the precipitate–matrix system per unit volume, respectively. K_β is a proportionality constant that depends on the density of homogeneous nucleation sites, the frequency at which single atoms join the critical nucleus, and the so-called Zeldovich factor [26].

For partitionless transformations, ΔG^β is the difference in the molar free energies of the phases normalized by the molar volume of the parent phase, V_m. For multi-component systems, the composition of the nucleus can deviate from that of the parent phase and additional terms must be considered. ΔG^β is expressed for a binary system in Eq. (2). X_β and $G_\beta(X)$ are the composition and molar free energy of the nucleated β-phase, while X_0 and $G_\delta(X)$ are the corresponding values for the parent δ-phase [16,27]:

$$\Delta G^\beta(X_0, X_\beta) = \frac{1}{V_m}\left[[G_\beta(X_\beta) - G_\delta(X_0)] - (X_\beta - X_0)\frac{\partial G_\delta(X)}{\partial X}\Big|_{X=X_0} \right] \quad (2)$$

Eq. (2) implicitly assumes a negligible change in the composition of the parent phase associated with the nucleation of a product phase of a different composition, an approximation most appropriate for the first nuclei to form. The equation is represented graphically as a function of X_β by the vertical distance between the line tangent to $G_\delta(X)$ at X_0 and the value of $G_\beta(X)$ evaluated at X_β (see Fig. 1a). The composition, X_β^*, of the nucleus with the maximum thermodynamic driving force for nucleation (Eq. (2)) satisfies the "parallel tangency" condition [27]:

$$\frac{\partial G_\beta(X)}{\partial X}\Big|_{X_\beta^*} = \frac{\partial G_\delta(X)}{\partial X}\Big|_{X_0} \quad (3)$$

Fig. 1a illustrates the parallel tangency condition and Fig. 1b illustrates the common tangency condition that dictates the compositions corresponding to two-phase equilibrium for comparison. The parallel tangency condition of Eq. (3) tends to promote chemical partitioning during nucleation in order to maximize the thermodynamic driving force. However, the strain and interface energy terms of Eq. (1) can also affect compositional partitioning in the case where they are dependent upon composition.

Phase selection during crystallization can be growth controlled, but here we assume nucleation control because growth would be similar for the bcc, fcc and hcp phases [15]. According to Eq. (1), the phase with the lowest ΔG_β^* and hence the highest steady-state nucleation rate would therefore be formed preferentially. Lower interface energies, lower strain energies and a larger thermodynamic driving force (ΔG^β) associated with nucleation can all promote preferential formation of a particular phase. ΔG^β is governed by volume free energies (Eq. (2)) and the phase with the lowest free energy at the nucleus composition would be the preferentially nucleated phase if the strain and interface energies could be neglected. The nucleus com-
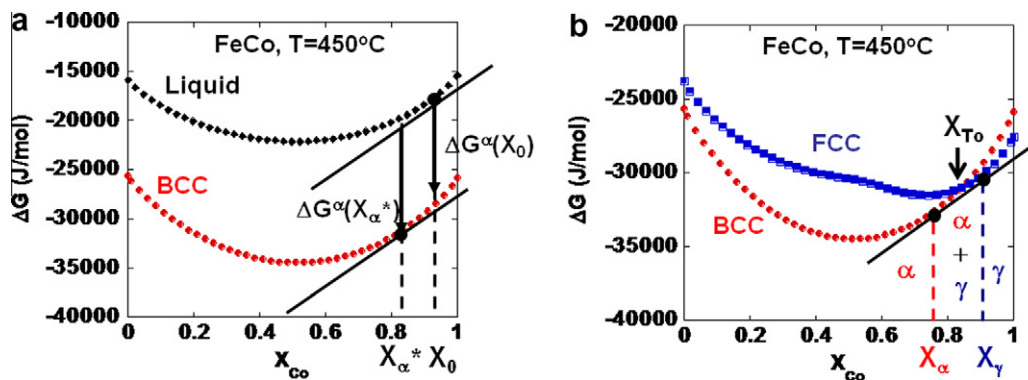
Fig. 1. (a) The thermodynamic driving force for nucleation represented graphically for nucleation of disordered bcc (α) from a hypothetical liquid phase at $T = 450\,°C$. X_0 = original liquid composition and X_α^* = bcc composition satisfying the parallel tangency condition. The vertical distance between the line tangent to the liquid phase at X_0 and the bcc free energy curve at a given nucleus composition, X_α, gives the corresponding thermodynamic driving force, $\Delta G^\alpha(X_\alpha)$. $|\Delta G^\alpha(X_\alpha^*)| > |\Delta G^\alpha(X_0)|$, as expected. (b) The common tangent construction dictating the compositions at the boundaries of the two-phase region (X_α and X_γ) between disordered bcc and fcc phases in the Fe–Co binary system at $T = 450\,°C$.

position at which two phases exhibit equal driving forces is the intersection of the free energy vs. composition curves, X_{T_0}, which corresponds to the well-known T_0 line [28].

In general, the strain and interface terms of Eq. (1) also contribute to the determination of the phase and composition of the nucleus with the lowest value of ΔG_β^*. Quantitative application of the model described here has been employed in a number of references to explain preferential nucleation of bcc phase for highly undercooled liquids in the Fe–Co, Fe–Ni and Fe–Cr–Ni systems [15–17,29–31] under conditions where fcc phase is expected to be stable. Strain terms are neglected as the transformation is from a liquid to a solid phase, but in many cases it is crucial to consider the interfacial term [16]. The solid–liquid interfacial energy was estimated from the molar entropy of fusion $(S_L(X_0, T) - S_\beta(X_\beta, T))$, the temperature (T), Avogadro's number (N_a), the molar volume of the melt (V_m) and a structure-dependent coefficient (α) based on the model of Spaepen et al. [32–34], as expressed in Eq. (4):

$$\sigma = \alpha \left(\frac{S_L(X_0, T) - S_\beta(X_\beta, T)}{(N_a)^{1/3}(V_m)^{2/3}} \right) T \qquad (4)$$

It is typically assumed that $\alpha_{bcc} \sim 0.71\text{–}0.76$ and $\alpha_{fcc} \sim \alpha_{hcp} \sim 0.86$. The interface energy thus tends to be lower for the bcc phase, thereby promoting nucleation of bcc when all other terms of Eq. (4) are similar.

The model of Spaepen et al. [32–34] deals with monatomic solids at the melting temperature, and Eq. (4) is not strictly correct for estimating the amorphous and crystalline interfacial energy for nucleation from an amorphous phase at relatively low temperatures. Additional complexities include the low atomic mobility in the amorphous phase below the glass transition temperature and chemical and magnetic ordering effects that strongly alter the entropies of each phase (directly used in Eq. (4)). Nevertheless, Eq. (4) has been used to estimate the amorphous–crystalline interfacial energy above the glass transition temperature [35] and the basic arguments underpinning Eq. (4)

have been employed to rationalize a tendency for the bcc phase to preferentially nucleate during crystallization of Fe,Ni-based amorphous precursors [36]. We therefore apply this expression below, though the detailed quantitative results should be treated with some caution.

For solid–solid nucleation processes the strain term of Eq. (1) must be considered, and we assume a hydrostatic strain of precipitation associated with the difference in molar volumes of the crystalline and amorphous phases. According to Nabarro [37], the following equation describes the strain energy of a hard precipitate forming in a soft matrix phase so that the majority of strain is accommodated in the matrix:

$$W^{\delta,\beta} = 6\mu V \varepsilon^2 \qquad (5)$$

In Eq. (5), μ is the shear modulus of the matrix, V is the volume of the precipitate and ε is a linear measure of the volume misfit between the matrix and the precipitate. The equation is applied in this work because the experimentally observed increase in the lattice parameter of bcc nanocrystals of $(Co,Fe)_{88}Zr_7B_4Cu_1$ alloys relative to bulk Co–Fe alloys would yield only a small $|\varepsilon| \sim 0.3\%$ as compared to the expected $|\varepsilon| \sim 2\text{–}3\%$ misfit between the amorphous precursor and the crystalline bcc phase [8,38]. For simplicity, we roughly approximate the shear modulus as that of pure Fe ($\mu \sim 80\,GPa$) and we estimate the volume misfit, ε, using theoretical densities from ab initio calculations of the bcc, fcc and simulated amorphous phases. Under these assumptions, the strain term would favor nucleation of the bcc phase relative to the closer-packed fcc and hcp phases. It has been argued that the hydrostatic strain effect can be reduced or even eliminated through accommodation by other means, such as vacancies [26], an enhanced content of dissolved glass formers in the crystalline phase or other defects such as dislocations. For crystallization from an amorphous phase, diffusional processes can relax the strain above the glass transition temperature. For the alloys discussed in this work, crystallization typically happens at

temperatures below which any evidence for the glass transition can be detected through standard calorimetric techniques.

3. Model results

The free energies of the liquid phase and the disordered bcc, fcc and hcp phases of the binary FeCo system [39,40] were taken from the BINARY SGTE Alloy Database using Thermocalc™. In Fig. 2, the free energy curves are presented as a function of composition for $T = 1400\,°C$ and $T = 450\,°C$, along with the most recent binary phase diagrams [41]. The former temperature is reasonable for solidification of a highly undercooled liquid, while the latter roughly corresponds to a temperature at which crystallization of amorphous (Fe,Co)-based precursors such as $(Co,Fe)_{89}Zr_7B_4$ is observed. Chemical ordering is expected in the bcc phase (B2-bcc derivative) for Co–Fe alloys at equilibrium for $T = 450\,°C$ but this effect is neglected here, an approximation valid for the most Co-rich alloys of primary interest.

3.1. Isothermal solidification of a liquid at $T = 1400\,°C$

As an illustration, the model is first applied to the isothermal solidification of a binary FeCo liquid at $T = 1400\,°C$ using the free energy curves of Fig. 2c. Isothermal nucleation is assumed but experiments are actually

carried out through finite cooling rates of small liquid droplets [16]. Estimated values of ΔG_β^* (Eq. (1)) for both the bcc (ΔG_α^*) and fcc (ΔG_γ^*) phases were calculated at $T = 1400\,°C$ with (Fig. 3a) and without (Fig. 3b) accounting for the interfacial energy term using Eq. (4). In Fig. 3, $X_{L,\alpha=\gamma}$ is the approximate X_{Co} of the parent liquid phase where $\Delta G_\alpha^* = \Delta G_\gamma^*$. The bcc phase would only be expected to preferentially nucleate (i.e. $\Delta G_\alpha^* < \Delta G_\gamma^*$) for very dilute Co-containing alloys if interfacial effects are neglected. Accounting for interfacial effects using Eq. (4), however, it is predicted that bcc should preferentially nucleate up to Co contents of roughly 30 at.%. Recent experimental work has verified this tendency [30].

3.2. Crystallization from an undercooled binary liquid at $T = 450\,°C$

Free energies of amorphous precursors are not well known, so we first apply the model to an undercooled binary FeCo liquid near the crystallization temperature as done previously [14]. The composition of each crystalline phase satisfying the parallel tangency condition (Eq. (3)) was calculated as a function of the supercooled liquid composition, as presented in Fig. 4a. For a given initial supercooled liquid composition on the horizontal axis in Fig. 4a, the corresponding composition satisfying the parallel tangency for each of the possible phases to nucleate can be read from the vertical axis. Chemical partitioning is pre-
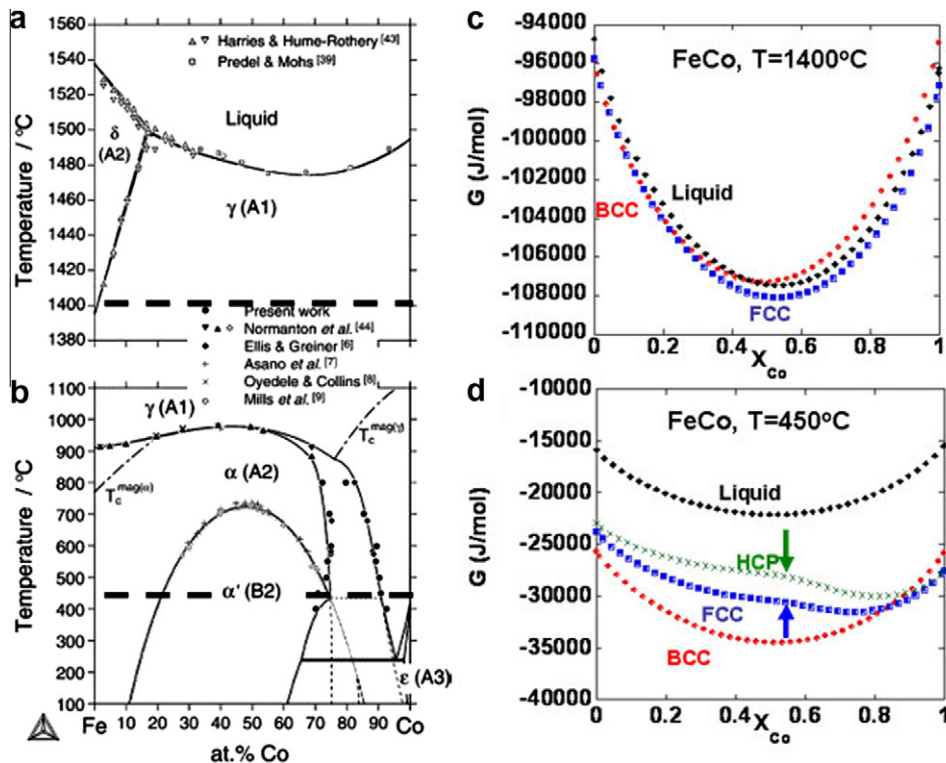

Fig. 2. (a) High temperature and (b) low temperature phase diagrams of the Fe–Co system [41], with the temperatures of interest highlighted with a dashed line. Free energy vs. composition curves of (c) bcc, fcc and liquid phases at $T = 1400\,°C$ and (d) disordered bcc, fcc, hcp and hypothetical liquid phases at $T = 450\,°C$. The vertical arrows indicate the compositions roughly corresponding to the onset of ferromagnetic order for fcc and hcp alloys.
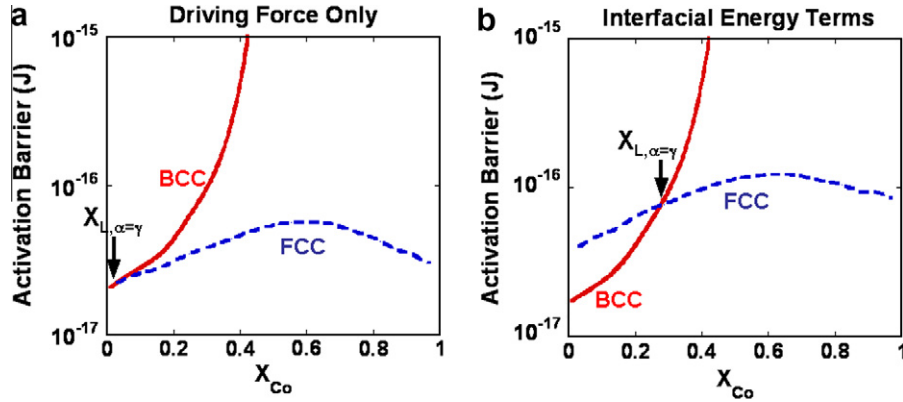
Fig. 3. ΔG_α^* and ΔG_γ^* calculated using Eq. (1) and the interfacial energy expression of Eq. (4) for isothermal nucleation at $T = 1400\,°C$. $X_{L,\alpha=\gamma}$ is the approximate X_{Co} of the parent liquid phase where $\Delta G_\alpha^* = \Delta G_\gamma^*$. (a) Dependence of the interfacial energy on the phase and composition is neglected. (b) The composition and phase-dependent interfacial energy of Eq. (4) is employed resulting in preferential nucleation of bcc phase.
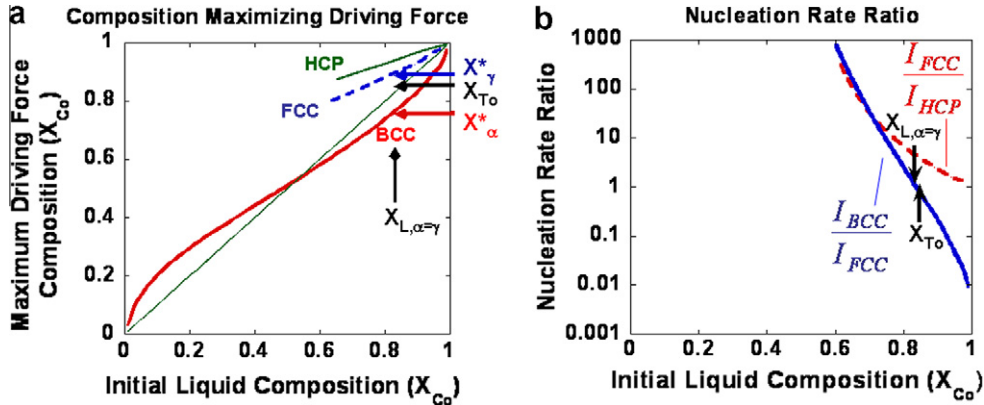

Fig. 4. (a) Composition of the bcc, fcc, and hcp phases that satisfy the parallel tangency condition for the hypothetical liquid phase at $T = 450\,°C$. The 45° line corresponds to no partitioning. (b) Ratio of steady-state nucleation rates of bcc/fcc and fcc/hcp estimated using the expressions of Eq. (3) and neglecting any composition and phase dependence of strain and interface terms. X_{T_0} = intersection of free energy curves of bcc and fcc at $T = 450\,°C$. $X_{L,\alpha=\gamma}$ = liquid composition where the nucleation rates are equal for the bcc and fcc nuclei that satisfy the parallel tangent condition (X_α^* and X_γ^*). Vertical arrows refer to supercooled liquid compositions, while horizontal arrows refer to compositions of the product phases.

dicted such that the composition of the first bcc phase to nucleate deviates towards an equiatomic Fe–Co composition due to the negative enthalpy of mixing of Fe and Co atoms even in the disordered bcc phase [2]. Allowing for chemical ordering in the crystalline phase would be expected to result in an even stronger tendency for partitioning towards the equiatomic composition. Partitioning of Co to fcc and hcp crystalline phases is predicted in Fig. 4a because of the relatively low free energy of Co-rich fcc and hcp phases (Fig. 2d).

In Fig. 4b, the calculated ratios of the bcc/fcc (I_{bcc}/I_{fcc}) and fcc/hcp (I_{fcc}/I_{hcp}) steady-state nucleation rates are presented (Eq. (1)), neglecting the strain terms and assuming that the interfacial energies are identical for both phases. Where $I_{bcc}/I_{fcc} = 1$, both bcc and fcc have an equal probability of nucleating from the hypothetical supercooled liquid. This supercooled liquid composition, $X_{L,\alpha=\gamma} \sim 0.83$, is close to expectations for a partitionless transformation, $X_{T_0} \sim 0.84$. However, Fig. 4a illustrates that the actual compositions of the most probable bcc and fcc nuclei to

form initially for a supercooled liquid of composition $X_{L,\alpha=\gamma}$ lie at significantly lower ($X_\alpha^* \sim 0.77$) and higher ($X_\gamma^* \sim 0.90$) Co contents, respectively.

Because of the similar free energies of bcc, fcc and hcp for high Co-containing alloys (see Fig. 2d), the estimated ratios of nucleation rates (I_{bcc}/I_{fcc} and I_{fcc}/I_{hcp}) lie within the range of 0.1–10 over a significant composition range (see Fig. 4b). This simple approximation would suggest that crystalline phases of various structures could nucleate in significant amounts over a wide composition range where only one phase is thermodynamically stable. Because the most probable compositions of each phase to nucleate would be given by Fig. 4a, one would also expect a monotonic variation in the composition of each phase as a function of the original alloy composition.

For comparison, the calculations of ΔG_α^* and ΔG_γ^* were repeated, including the interface (Eq. (4)) and strain (Eq. (5)) terms, but neglecting the effects of strain and interface energy on nucleus composition. The latter simplification is appropriate due to the uncertainties in the quantitative esti-

mates of these terms, as noted in the introduction, and we have verified that it does not qualitatively alter the major predictions discussed below. It is noted that the strain term would be irrelevant for nucleation from an undercooled liquid, but we include the term here to yield insight about the magnitude of the effect under an assumption that the amorphous phase could be reasonably modeled as an undercooled liquid.

The calculated values of ΔG_α^* and ΔG_γ^* are presented in Fig. 5. In Fig. 5a the interface and strain terms are assumed to be the same as those used in generating Fig. 4. In Fig. 5b, Eq. (4) is used to estimate a solid–liquid interfacial energy (entropies of Fig. 5d, $\alpha_{bcc} = 0.72$, and $\alpha_{fcc,hcp} = 0.86$) and in Fig. 5c, Eq. (5) is used to estimate the strain of precipitation for crystallization from an amorphous precursor rather than a melt. Estimates of $\varepsilon \sim -2.3\%$ for bcc Co and $\varepsilon \sim -2.8\%$ for fcc Co were obtained using theoretical densities of simulated $(Co,Fe)_{89}Zr_7B_4$ amorphous alloys (discussed in subsequent section) corresponding to $W^{Liq \rightarrow bcc} \sim 29.0$ J g^{-1} and $W^{Liq \rightarrow fcc} \sim 44.1$ J g^{-1}. These values are significant compared to estimated thermodynamic driving forces for nucleation based on the free energy curves ($\Delta G^\beta \sim 100$–200 J g^{-1}), suggesting that strain effects could play a significant role in phase selection during nucleation for these systems.

Fig. 5b and c demonstrates that both the strain and interface energy terms result in a strong tendency for preferential nucleation of bcc. The former is predicted to result in the preferential nucleation of the bcc phase even in alloys with no Fe, while the latter is predicted to result in a shift of $X_{L,\alpha=\gamma}$ to Co contents as high as $X_{Co} \sim 0.95$. The composition range over which multiple phases would be expected to nucleate is also significantly reduced compared to the predictions of Fig. 4b, which accounted for only the driving force terms. By comparison with the values calculated in Fig. 4a, the bcc composition most likely to nucleate corresponding to the value of $X_{L,\alpha=\gamma}$ in Fig. 5c is $X_\alpha^* \sim 0.91$. This value is significantly enriched in Co relative to $X_{T_0} \sim 0.84$, which is an illustration that classical nucleation theory can account for preferentially nucleated bcc phase with $X_\alpha^* > X_{T_0}$ when strain and/or interface terms are taken into account.

It should be noted that accounting for the interfacial energy term using Eq. (4) results in predictions of $\Delta G_\alpha^* > \Delta G_\gamma^*$ for a range of Fe-rich alloys which is not consistent with experiments in real systems. This incorrect prediction results from a large entropy of fcc relative to the bcc phase at this temperature (see Fig. 5d) due to magnetic ordering effects. The end result is a small estimated interfa-
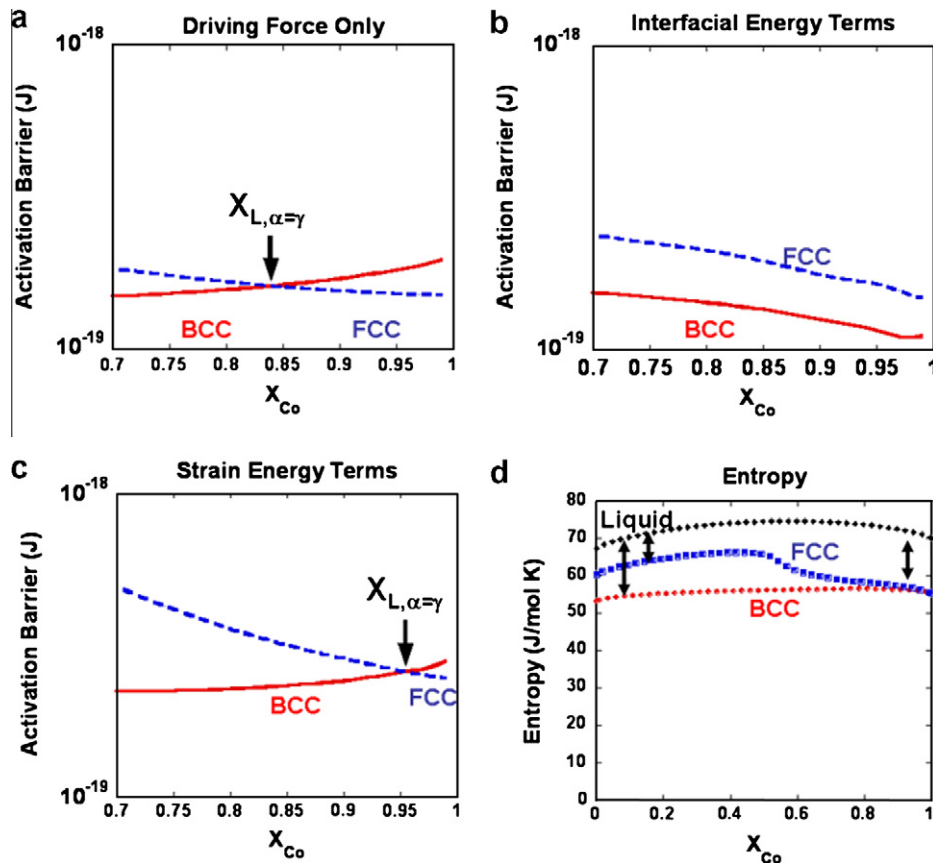

Fig. 5. ΔG_α^* and ΔG_γ^* as functions of composition for the Co-rich alloys accounting for (a) compositional partitioning to maximize the driving force, (b) the driving force and the interfacial energy expression of Eq. (4) and (c) the driving force and the strain energy term of Eq. (5). $X_{L,\alpha=\gamma}$ is the approximate X_{Co} of the parent liquid phase where $\Delta G_\alpha^* = \Delta G_\gamma^*$. In (d) the entropies of the bcc, fcc and hypothetical liquid phases are presented, showing an increase in entropy for Fe-rich fcc alloys due to the lack of ferromagnetic order.

cial energy of fcc as compared to the bcc phase according to Eq. (4), thereby promoting nucleation of fcc phase. For the Co-rich alloys of interest here both phases exhibit ferromagnetic ordering and are far below their respective Curie temperatures, so this complication does not arise. Nevertheless, as noted in the introduction, we suggest that this expression is not strictly valid for crystallization at such low temperatures, particularly when chemical and magnetic ordering effects are observed.

3.3. Crystallization from "amorphous" at T = 450 °C

The $(Co,Fe)_{89}Zr_7B_4$ alloy systems are actually complex multi-component systems rather than simple binary systems where the amorphous phase can be approximated well as an undercooled binary liquid. For a general N-component alloy, the composition can be described as a vector in a finite region of an $(N-1)$-dimensional space defined by Eq. (6). The expression for ΔG^β of Eq. (2) and the "parallel tangency" condition of Eq. (3) are generalized to Eqs. (7) and (8), respectively:

$$\vec{X} = \{X_1, X_2, \ldots, X_{N-1}\}, \quad \sum_{i=1}^{N} X_i = 1 \qquad (6)$$

$$\Delta G^\beta(\vec{X}_0, \vec{X}_\beta) = [G_\beta(\vec{X}_\beta) - G_\delta(\vec{X}_0)] - \vec{\nabla} G_\delta(\vec{X}_0) \cdot (\vec{X}_\beta - \vec{X}_0)$$
$$= [G_\beta(\vec{X}_\beta) - G_\delta(\vec{X}_0)] - \sum_{i=1}^{N-1} (X_{\beta,i} - X_{0,i}) \frac{\partial G_\delta(\vec{X})}{\partial X_i}\Big|_{\vec{X}=\vec{X}_0} \qquad (7)$$

$$\vec{\nabla} G_\beta(\vec{X})\Big|_{\vec{X}_\beta^*} = \vec{\nabla} G_\delta(\vec{X})\Big|_{\vec{X}_0} \qquad (8)$$

By neglecting any solubility of the glass-former species in the crystalline phase and treating the glass formers as a single species for simplicity, the system can be modeled as "pseudo-ternary" and the stoichiometric formula of the alloy can be expressed as $Fe_{X_{Fe}}Co_{X_{Co}}(Zr,B)_{X_{GF}}$. By a change of variables we can represent the stoichiometric formula of the alloy as $(Fe_x Co_{1-x})_{1-X_{GF}}(Zr,B)_{X_{GF}}$, where $1-x = X_{Co}/(X_{Fe} + X_{Co})$ is analogous to the mole fraction of Co in a binary Co–Fe alloy. Eqs. (6)–(8) now take the form of Eqs. (9)–(11):

$$\vec{X} = \{X_{Co}, X_{GF}\} \rightarrow \{x, X_{GF}\}, \quad X_{Fe} + X_{Co} + X_{GF} = 1 \qquad (9)$$

$$\Delta G^\beta(\vec{X}_0, x_\beta) = [G_\beta(x_\beta) - G_\delta(\vec{X}_0)] - \left(\frac{x_\beta}{1-X_{0,GF}} - x_0\right)$$
$$\times \frac{\partial G_\delta(\vec{X})}{\partial x_\delta}\Big|_{\vec{X}=\vec{X}_0} + X_{0,GF} \frac{\partial G_\delta(\vec{X})}{\partial X_{GF}}\Big|_{\vec{X}=\vec{X}_0} \qquad (10)$$

$$\frac{\partial G_\beta(x_\beta)}{\partial x_\beta}\Big|_{x_\beta^*} = \frac{1}{(1-X_{0,GF})} \frac{\partial G_\delta(\vec{X})}{\partial x_\delta}\Big|_{\vec{X}=\vec{X}_0} \qquad (11)$$

Similar to the binary case, the phase with the lowest free energy will have the largest thermodynamic driving force,

ΔG^β, for the formation of a nucleus of that composition. For the "pseudo-ternary" approximation, the crystalline phase with the largest value of ΔG^β for a given nucleus composition is still dictated by the binary free energy curves of the competing product phases. This conclusion remains true even for an amorphous precursor with a larger number of glass-former species if the solubilities of all of these species are negligible in the crystalline phase. Therefore, the discussion above regarding the importance of the X_{T_0} composition for nucleation in binary systems applies to the more complex "pseudo-ternary" systems as well.

To obtain a qualitatively reasonable estimate of the free energy of the amorphous precursors of composition $(Fe,Co)_{89}Zr_7B_4$, we have generated bcc supercells and amorphous structures of varying Co:Fe ratio and compared their ground state cohesive energies at fixed values of $x = X_{Fe}/(X_{Fe} + X_{Co})$ through ab initio theoretical techniques. In this way, we can estimate the enthalpy difference between the bcc phase and the amorphous phase at $T = 0$ K. The details of these calculations and ambiguities in this approach associated with the difference in the composition of the bcc and amorphous phase for fixed values of x are discussed in the Appendix. To justify the results of these calculations, we have also experimentally estimated the enthalpy of primary crystallization for $(Co_{1-x}Fe_x)_{89}Zr_7B_4$ and $(Co_{1-x}Fe_x)_{88}Zr_7B_4Cu_1$ alloys using differential scanning calorimetry (DSC), as presented in Fig. 6a and b. Considering that the experimental and theoretically estimated enthalpies do not correspond to identical transformations (see Appendix), similar qualitative trends and values of the same order of magnitude provide us with confidence that the qualitative trends observed are representative of the relative stability of the amorphous phase. The qualitative agreement is better if the bcc phase is assumed to have the maximum long-range chemical order possible (CsCl-type) at each composition. Both the theoretically and experimentally estimated enthalpies suggest that the amorphous phase is relatively more stable with respect to the crystalline phases that form during primary crystallization for the Co-rich alloys as compared to the Fe-rich alloys.

Using the ΔH values of Fig. 6b, the free energy of the disordered bcc phase was supplemented with an additional term to estimate the free energy of the amorphous precursors. Because of the unknown entropy of the amorphous precursors, two simplifying assumptions were employed. Neither assumption is strictly valid, but the goal is only to obtain reasonable estimates of the free energy of the amorphous phase such that they agree with the qualitative trends implied by the estimated enthalpies of primary crystallization.

Assumption 1. The specific heats of the liquid, amorphous, and crystalline phases are equal.

Assumption 1 is commonly employed in the calculation of thermodynamic driving forces from enthalpy data when incomplete information is available [42].
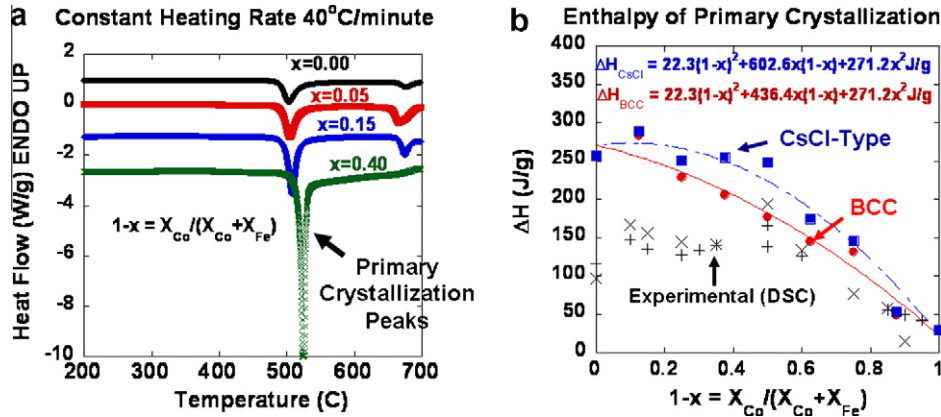
Fig. 6. (a) Constant heating rate (40 K min^{-1}) DSC experiments used for experimental enthalpy measurements of primary crystallization through integration of the area of the low temperature peak observed. (b) A comparison between experimental (Xs = $(Co_{1-x}Fe_x)_{88}Zr_7B_4Cu_1$ alloys, +s = $(Co_{1-x}Fe_x)_{89}Zr_7B_4$ alloys) and theoretical enthalpies (square = compared with maximally ordered Cs-Cl type, circle = compared with disordered bcc) estimated for primary crystallization as a function of x. Fits to the theoretical enthalpies are also presented graphically (disordered bcc = solid, CsCl-type = dashed).

Assumption 2. $(G_\alpha - G_{Amorphous})/\Delta H_{Amorphous \to \alpha} = (G_\alpha - G_{Liquid})/\Delta H_{Liquid \to \alpha}$ for each Co:Fe ratio at the temperature of interest.

Assumption 2 is not a standard assumption but, in conjunction with Assumption 1, it can be loosely interpreted that the amorphous phase, crystalline phase and liquid phase all have equal free energies for a given Co:Fe ratio at the melting temperature, T_M. By using Assumptions 1 and 2, one can obtain an estimate for $(G_\alpha - G_{Amorphous})$ based on enthalpy data alone.

The estimated free energy difference between the amorphous $(Co_{1-x}Fe_x)_{89}Zr_7B_4$ phase and the disordered bcc phase exhibits the same qualitative trend with composition as the theoretically estimated enthalpies of primary crystallization in Fig. 6b. The estimated free energy curve for the amorphous phase presented in Fig. 7a (obtained using the

theoretical enthalpy values of Fig. 6b) is also reasonable in magnitude as it is lower than the binary liquid phase and higher than the equilibrium binary crystalline phases across the entire composition range. Therefore, the free energy curves of Fig. 7a are sufficient to illustrate how the compositional dependence of the free energy of the amorphous phase can affect the compositional partitioning behavior in the framework of classical nucleation theory.

Fig. 7b presents the compositions that maximize the driving force for nucleation for both the bcc and fcc phases using the modified parallel tangency condition of Eq. (11) and the estimated free energy of the amorphous phase calculated as described above. Results are illustrated for calculations using both the theoretical and experimental enthalpies in Fig. 6b. For the $(Co_{1-x}Fe_x)_{89}Zr_7B_4$ system, a tendency for partitioning of Fe to the bcc crystalline phase even for near-equiatomic alloys ($x \sim 0.5$) is now predicted
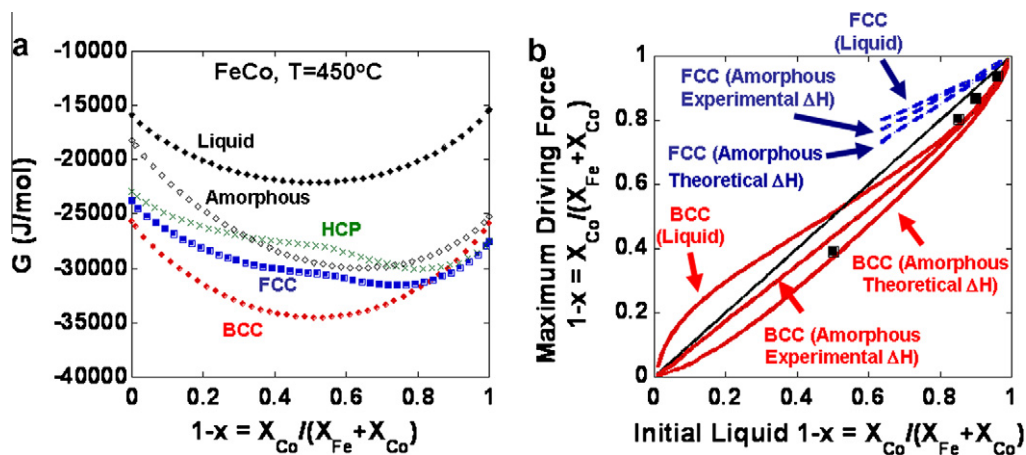

Fig. 7. (a) Free energy curves reproduced from Fig. 2d and the estimated free energy of the amorphous $(Co_{1-x}Fe_x)_{89}Zr_7B_4$ phase (open diamonds) as a function of $(1 - x)$ using the disordered bcc theoretical enthalpy of Fig. 6b. (b) A comparison between the predicted compositional partitioning of bcc and fcc to maximize the thermodynamic driving force for nucleation using the free energy of the hypothetical binary liquid and the amorphous phase free energy estimated from both the theoretical and experimental enthalpies of Fig. 6b. In (b), the large squares correspond to experimental data points obtained for the bcc phase using 3DAP for "nanocomposite" $(Co_{1-x}Fe_x)_{89}Zr_7B_4$ or $(Co_{1-x}Fe_x)_{88}Zr_7B_4Cu_4$ alloys [8,25].

which is consistent with the current published experimental results obtained with 3DAP, as indicated in Fig. 7b for comparison [8,25]. This trend has been explained previously [25] based on the argument that the Co–Zr pair interaction is stronger than the Fe–Zr pair interaction. In the context of the current model, this simple argument would be used to justify the smaller enthalpy of crystallization for Co-rich alloys, as shown in Fig. 6b, and the smaller estimated free energy difference between the Co-rich amorphous alloys and the bcc crystalline phase in Fig. 7a. For comparison, we have also included calculations using the experimentally measured enthalpies in Fig. 7b. The resultant asymmetry in the partitioning behavior for Fe-rich vs. Co-rich alloys is presumably associated with the experimentally observed chemical ordering of the bcc crystalline phase that would tend to promote partitioning toward an equiatomic Fe:Co ratio. These calculations illustrate that the free energy of the amorphous phase can play a significant role in the chemical partitioning during crystallization. Therefore, the compositional partitioning of Fe and Co atoms to the crystalline phase is expected to depend upon the identity and quantity of glass formers even when the glass forming elements are completely insoluble in the crystalline phases that form.

In a more general case, a significant content of glass-former species could be dissolved into the nucleated crystalline phases, thereby stabilizing one of the primary crystalline phases, as compared to expectations based on the free energies of the binary Fe–Co system. Consequently, the generalized expressions of Eqs. (6)–(8) would be the applicable ones governing the maximization of the thermodynamic driving force. In such cases, X_{T_0} estimated from the binary free energy curves may no longer be relevant and values of $(1-x) > X_{T_0}$ for a preferentially nucleated bcc phase could be observed in such complex systems based on thermodynamic driving force considerations alone. As noted previously [8,25], the dissolved content of B and Zr in the Fe,Co nanocrystals of the $(Co_{1-x}Fe_x)_{89}Zr_7B_4$ alloys is larger than the bulk solubility would predict, and this effect cannot be completely excluded.

4. Conclusions

Steady-state classical nucleation theory has been applied to Co-rich Fe,Co-based alloys under a number of simplifying assumptions. This simple theory offers some explanations for experimental observations noted in the introduction for crystallization of $(Fe,Co)_{89}Zr_7B_4$ and $(Fe,Co)_{89}Zr_7B_4Cu_1$ amorphous precursors.

Observation 1. The strain and/or interface energy effects could be significant enough to account for the preferential nucleation of the bcc phase with Co:(Fe + Co) ratios $>X_{T_0}$ of the binary bcc and fcc bulk free energy curves. Zr and B are insoluble in bulk binary Fe–Co crystalline phases but are found in the nanocrystals in significant amounts after crystallization ($\sim$2–4% of each), which could also potentially stabilize the bcc phase.

Observation 2. The presence of multiple nanocrystalline phases of similar free energies after crystallization in composition and temperature ranges where only the fcc phase is predicted to be stable in the binary Fe–Co system could be attributed to the statistical nature of nucleation.

Observation 3. The compositions of the nucleated nanocrystals are not governed by the equilibrium common tangency condition and so they demonstrate monotonically varying Co:(Co + Fe) ratios with the corresponding value of the initial amorphous precursor even when multiple phases are nucleating. The parallel tangency condition of the classical nucleation theory displays this behavior.

Observation 4. Fe-enrichment of bcc phase for both Co-rich and near-equiatomic alloys could be due to the smaller free energy difference between the amorphous phase and the bcc nanocrystalline phase for high Co-containing alloys.

If strain and/or interface energy effects are the dominant factors promoting preferential nucleation of bcc in the $(Co_{1-x}Fe_x)_{89}Zr_7B_4$ alloys of particular interest (Observation 1), then this phenomenon should be observed as a general trend during crystallization of amorphous precursors when a bcc phase is competing with close-packed phases such as fcc and hcp. The situation would be analogous to the tendency for the preferential nucleation of the bcc phase observed in the nucleation experiments of highly undercooled Fe–Co, Fe–Ni, and Fe–Ni–Cr liquid droplets.

Acknowledgements

Appendix A

Ab initio calculations of the theoretical enthalpy change between the bcc phase $(Co_{1-x}Fe_x)$ and the amorphous phase $((Co_{1-x}Fe_x)_{89}Zr_7B_4)$ were performed using supercells of $2 \times 2 \times 2$ conventional unit cells for bcc and by simulating reasonable amorphous structures through molecular dynamics techniques, as in previous work [43]. The Vienna Ab-Initio Simulation Package (VASP) was used with a Projector-Augmented Wavefunction basis set and a spin-polarized Generalized Gradient Approximation exchange–correlation function.

The initial amorphous structure consisted of a previously annealed amorphous structure of 100 atoms (45 Fe, 44 Co, 7 Zr and 4 B) quenched to low temperatures [43]. We then substituted Fe and Co atoms into the structure randomly to vary the Fe–Co stoichiometry and the structures were relaxed using conjugate gradient relaxation with a single electronic *k*-point (gamma point). Once the residual forces were low and the cohesive energies converged to less than 1 meV atom^{-1} after 10 subsequent ionic relaxation steps, the structures were re-relaxed using a $2 \times 2 \times 2$ *k*-point mesh. The relaxation steps were followed by a single static calculation from which the calculated cohesive energies used to estimate the enthalpies were reported.

Supercells of the bcc structure ($2 \times 2 \times 2$ conventional unit cells) were generated with varying amounts of Co and Fe atoms. The atoms were placed to result in both a zero long-range chemical order parameter (disordered bcc) and a maximally chemically ordered structure (CsCl-type) for each composition. The structures were then relaxed self-consistently to determine the ground state cohesive energy and the spin-polarized electron density at $T = 0$ K.

The difference in composition between the amorphous and crystalline phases for the same Co:Fe ratio cause an ambiguity in defining a theoretical enthalpy of primary crystallization as the experimental and theoretical reactions are not identical. The relevant transformations for each of the series plotted in Fig. 6 are as follows:

Theoretical : Amorphous $(Fe_xCo_{1-x})89Zr_7B_4$

$\rightarrow (Fe_xCo_{1-x}) - CsCl$ or bcc $+ ZrB_2 + Zr$

Experimental : Amorphous1 $(Fe_xCo_{1-x})89Zr_7B_4$

$\rightarrow (Fe, Co) - CsCl$ or bcc $+$ Amorphous 2

Experimentally, a second amorphous phase of different composition is present after the first crystallization step, partitioning of Fe occurs between the amorphous and crystalline phases, and fcc/hcp phase is also observed for the highest Co-containing alloys. Theoretically, crystallization was approximated by a complete transformation of the amorphous precursor to bcc or CsCl-type Fe,Co and the most stable Zr and B crystalline phases. Nevertheless, the correspondence between the theoretical and experimental enthalpies of Fig. 6 strongly suggests that the Co-rich amorphous precursors are more stable than the Fe-rich compositions with respect to a primary crystalline bcc phase that forms during primary crystallization.

References

[1] Yoshizawa Y, Oguma S, Yamauchi K. J Appl Phys 1988;64:6044.
[2] McHenry MA, Willard MA, Laughlin DE. Prog Mater Sci 1999;44:291–433.
[3] Makino A, Suzuki K, Inoue A, Masumoto T. Mater Trans, JIM 1991;32:551–6.
[4] Willard MA, Laughlin DE, McHenry ME, Thoma D, Sickafus K, Cross JO, et al. J Appl Phys 1998;84:6773–5.
[5] Herzer G. IEEE Trans Mag 1990;26:1397–402.
[6] Ohodnicki PR. Thesis, Materials Science and Engineering Department, Carnegie Mellon University; 2008.
[7] Ohodnicki PR, Park SY, McWilliams HK, Ramos K, Laughlin DE, McHenry ME. J Appl Phys 2007;101:09–108.
[8] Ohodnicki PR, Qin YL, Laughlin DE, McHenry ME, Kodzuka M, Ohkubo T. Acta Mater 2009;57:87–96.
[9] Ohodnicki PR, Qin YL, Laughlin DE, McHenry ME, Keylin V. J Magn Magn Mater 2010;322:315–21.
[10] Ohodnicki PR, Long J, Laughlin DE, McHenry ME, Keylin V. J Appl Phys 2008;104:113909.
[11] Yoshizawa SFY, Ping DH, Ohnuma M, Hono K. Scripta Mater 2003;48:863–8.
[12] Yoshizawa SFY, Ping DH, Ohnuma M, Hono K. Mater Sci Eng A 2004;375–377:207–12.
[13] Yoshizawa Y, U.S. Patent 6648990 B2. United States of America: Hitachi Metals Limited; 2003.
[14] Willard M, Heil T, Goswami R. Metall Mater Trans A 2007;38:725–31.
[15] Li M, Ozawa S, Kuribayashi K. Philos Mag Lett 2004;84:483–93.
[16] Volkmann T, Herlach D, Löser W. Metall Mater Trans A 1997;28:453–60.
[17] Eckler K, Gartner F, Assadi H, Norman AF, Greer AL, Herlach DM. Mater Sci Eng A 1997;226–228:410–4.
[18] Li M, Yang G, Zhou Y. J Mater Sci 2000;35:3069–75.
[19] Yeon-Wook K, Hong-Ming L, Kelly TF. Acta Metall 1988;36:2525–36.
[20] Hong-Ming L, Yeon-Wook K, Kelly TF. Acta Metall 1988;36:2537–50.
[21] Kelton KF. J Non-Cryst Solids 2000;274:147–54.
[22] Kelton KF. Acta Mater 2000;48:1967–80.
[23] Kelton KF. J Non-Cryst Solids 2003;317:71–7.
[24] Diao J, Salazar R, Kelton KF, Gelb LD. Acta Mater 2008;56:2585–91.
[25] Ping DH et al. Scripta Mater 2001;45:781–6.
[26] Aaronson H, editor. Lectures on the theory of phase transformations. New York: The Metallurgical Society of AIME; 1975.
[27] Hillert M. In: Aaronson H, editor. Lectures on the theory of phase transformations. Warrendale, PA: The Minerals, Metals, & Materials Society; 1999.
[28] Massalski TB. In: Proceedings of the fourth international conference on rapidly quenched metals; 1981. p. 203–08.
[29] Perepezko JH. Mater Sci Eng: A 2005;413–414:389–97.
[30] Li M, Song G, Yang G, Hou Y. J Mater Res 1999;14:1679–82.
[31] Yeon-Wook K, Kelly TF. Acta Metall Mater 1991;39:3237–49.
[32] Spaepen F. Acta Metall 1975;23:729–43.
[33] Spaepen F, Meyer RB. Scripta Metall 1976;10:37–43.
[34] Spaepen F. Solid State Phys – Adv Res Appl 1994;47:1–32.
[35] Thompson CV, Greer AL, Spaepen F. Acta Metall 1983;31:1883–94.
[36] Greer AL, Walker IT. In: Transformations in primary crystallites in (Fe,Ni)-based metallic glasses. Ann Arbor, MI: Trans Tech Publications; 2002. p. 77–88.
[37] Nabarro FRN. In: Proceedings of the royal society of London, vol. 175; 1940. p. 519–38.
[38] Johnson F, Thesis, Materials Science and Engineering Department, Carnegie Mellon University; 2003.
[39] Guillermet AF. High Temp High Pres 1988;19:477–99.
[40] Guillermet AF. TRITA-MAC 1986;324.
[41] Ohnuma I, Enoki H, Ikeda O, Kainuma R, Ohtani H, Sundman B, et al. Acta Mater 2002;50:379–93.
[42] Thompson CV, Spaepen F. Acta Metall 1979;27:1855–9.
[43] Ganesh P, Widom M. Phys Rev B (Cond Matter Mater Phys) 2008;77:014205–10.